JGR Atmospheres

RESEARCH ARTICLE
10.1029/2020JD032827

Special Section:
A New Era Of Lightning Observations From Space

Evaluating Geostationary Lightning Mapper Flash Rates Within Intense Convective Storms

S. A. Rutledge[1], K. A. Hilburn[2], A. Clayton[1], B. Fuchs[3], and S. D. Miller[2]

[1]Department of Atmospheric Science, Colorado State University, Fort Collins, CO, USA, [2]Cooperative Institute for Research in the Atmosphere, Colorado State University, Fort Collins, CO, USA, [3]WeatherFlow, Inc., Scotts Valley, CA, USA

Key Points:

- Geostationary Lightning Mapper (GLM) detection efficiency (DE) is characterized using Lightning Mapping Arrays
- Reduced detection efficiency (DE) is found for storms with anomalous charge structures
- Additional factors related to viewing geometry and day-night effects are likely required to explain regional differences in DE

Correspondence to:
S. A. Rutledge,
srutledg@colostate.edu

Citation:
Rutledge, S. A., Hilburn, K. A., Clayton, A., Fuchs, B., & Miller, S. D. (2020). Evaluating Geostationary Lightning Mapper flash rates within intense convective storms. *Journal of Geophysical Research: Atmospheres*, *125*, e2020JD032827. https://doi.org/10.1029/2020JD032827

Received 30 MAR 2020
Accepted 15 JUN 2020
Accepted article online 20 JUN 2020

Author Contributions:
Conceptualization: S. A. Rutledge, B. Fuchs, S. D. Miller
Formal analysis: S. A. Rutledge, K. A. Hilburn, A. Clayton, S. D. Miller
Funding acquisition: S. A. Rutledge
Investigation: S. A. Rutledge, K. A. Hilburn
Methodology: K. A. Hilburn, A. Clayton, B. Fuchs
Project administration: S. A. Rutledge
Software: K. A. Hilburn, A. Clayton, B. Fuchs
Supervision: S. A. Rutledge
Validation: S. A. Rutledge, K. A. Hilburn, A. Clayton, S. D. Miller
Writing - original draft: S. A. Rutledge
(continued)

Abstract The Geostationary Lightning Mapper (GLM) marks the first time that lightning observations at storm-scale resolution are operationally available from geostationary orbit. We evaluate GLM detection efficiency (DE) for a special class of convective storms characterized by anomalous charge structures. These storms are anomalous as their internal layered charge structure departs from the tripole charge structure model, where midlevel negative charge is situated between upper and lower positive charge layers. Anomalous storms are characterized by extreme flash rates, low median flash heights, and intense precipitation. Ground truth information on lightning flash rates is provided by Lightning Mapping Arrays (LMA), which measure VHF radio frequency emissions produced by electrical breakdown. This study contrasts two regions: Colorado, where electrically "anomalous" storms are numerous, and Alabama, where they are rare. This study analyzes GLM DE as a function of the precipitation water path, cloud water path, and lightning properties from LMA. The GLM DE is found to vary with the geometric size of the flash and with cloud water path, the latter depending on flash height and cloud water content. Optical scattering (attenuation) by precipitation-sized particles does not appear to be a factor since precipitation particles contain much less surface area than cloud particles. The size of the flash is correlated with its optical brightness, and the cloud water path is correlated with optical extinction. Regional differences in GLM DE remain that appear to be related to sensor viewing geometry and day versus night sensitivity differences.

1. Introduction

In 2016, an exciting new era for spaceborne observations of lightning began with the launch of the Geostationary Lightning Mapper (GLM; Goodman et al., 2013) as the first member of the Geostationary Operational Environmental Satellite R-series (GOES-R, named GOES-16). A second GLM is operational on GOES-S (GOES-17), launched in 2018. The GOES-R series satellites also carry the new Advanced Baseline Imager (ABI; Schmidt et al., 2017), a passive imaging radiometer that measures shortwave visible to thermal infrared (IR) properties across 16 broad spectral bands in the electromagnetic wavelength range of 0.4 to 14 μm.

Four low earth-orbiting optical lightning sensors preceded GLM, the Fast on-Orbit Recording of Transient Events (FORTE; Jacobson et al., 1999), the Optical Transient Detector (OTD; Christian et al., 2003), the Lightning Imaging Sensor on the NASA TRMM satellite (LIS; Kummerow et al., 1998, Mach et al., 2007), and, most recently, another LIS instrument on the International Space Station. Since the release of the first GLM data in spring 2017, studies have presented general aspects of GLM-detected lightning (Rudlosky, Goodman, & Virts, 2019; Rudlosky, Goodman, Virts, & Bruning, 2019), evaluated the detection efficiency of GLM relative to the Earth Networks Total Lightning Network (ENTLN, Marchand et al., 2019), described extremely large lightning flashes in the stratiform regions of Mesoscale Convective Systems (Bruning et al., 2019; Lyons et al., 2019; Peterson, 2019), examined the sensitivity of parameters used in the algorithm that merges lightning "groups" into flashes (Mach, 2020), and assessed GLM detection using LIS and Lightning Mapping Array data (Zhang & Cummins, 2020; hereafter, ZC20). Rudlosky, Goodman, and Virts (2019) showed that GLM clearly depicts the seasonal march of lightning across the Equator and that spatial patterns of GLM lightning were consistent with previous studies (for example, the land-ocean contrast in lightning flash rates). Peterson (2019) described hemispheric lightning flash rates and described an extremely large GLM-detected lightning flash with a length of 673 km.

Writing – review & editing: S. A. Rutledge, K. A. Hilburn, A. Clayton, B. Fuchs, S. D. Miller

In the Marchand et al. (2019) study, flashes from GLM were compared to ENTLN detected flashes to estimate the detection efficiency (DE; ratio of GLM to ENTLN flashes) over a restricted area and time window. DE was found to be highest over the southeast United States with a local minimum over the Western and Northern Great Plains. These areas of the Great Plains are locations where anomalous storms (from an electrical perspective) occur with considerable frequency (Fuchs et al., 2016; Zajac & Rutledge, 2001). Marchand et al. argued that this regional DE reduction may be due to subpixel-scale flashes and optical attenuation of flashes, the latter amplified in anomalous storms that have low mean flash heights and significant precipitation and cloud water contents (Fuchs et al., 2018; Fuchs & Rutledge, 2018).

Important results regarding GLM detection efficiency were reported by ZC20. Using data from the Kennedy Space Flight Center Lightning Mapping Array, they demonstrated the GLM mean daily flash detection efficiency to be above 70%, meeting the instrument specification detection efficiency (Goodman et al., 2013). ZC20 found that the detection efficiency decreased as flashes became physically shorter in space and time, dropping to 20–40% for high flash rate storms in Florida. Conversely, flashes larger than a few tens of kilometers in length were detected with near 100% efficiency. Accordingly, ZC20 reported that detection efficiencies were higher for cloud-to-ground flashes compared to intracloud discharges, even though the latter are far closer to cloud top. Cloud-to-ground flashes were evidently well detected due to their large length and high channel luminosity, leading ZC20 to include that GLM DE depends on both quantities. The results presented in this study compliment this previous research.

Similar to ZC20, we employ VHF Lightning Mapping Array observations (LMA; Rison et al., 1999) to evaluate GLM detection efficiencies for several case studies over Colorado and Alabama. These two regions are selected given the availability of radar and LMA data and since they provide a contrast in storm type between "normal" polarity storms in AL and anomalous storms in CO (normal versus anomalous polarity storms will be discussed in more detail below). The comparison between GLM flashes and LMA flashes is inherently difficult, as flash rates are compared between optical energy emitted by lightning (photons arriving at the GLM sensor) against VHF-based radio frequency emissions produced by local electrical breakdown along lightning channels. However, lightning flash rate estimations based on LMA are considered the "gold standard" (Thomas et al., 2004. Fuchs & Rutledge, 2018, and references therein).

Three detailed case studies are first discussed. Two of these cases are anomalous storms (Bruning et al., 2014; Fuchs et al., 2018), which may feature an inverted, anomalous charge structure, or an inverted dipole structure with positive charge situated below negative charge. This latter situation is especially conducive to low mean flash heights. Since anomalous storms form in semiarid environments, cloud bases are high, and cloud updraft regions are wide, both which work to reduce entrainment and promote large supercooled liquid water contents (Fuchs et al., 2018). Large supercooled cloud water contents, promoting large rime accretion rates by graupel, is considered a necessary condition for imparting positive charge to graupel particles (Avila & Pereyra, 2000; Saunders & Peck, 1998; Takahashi, 1978).

Anomalous storms are intense storms, accompanied by very large flash rates, typically exceeding 100 flashes min^{-1} (Fuchs et al., 2015). Within the United States, about 10% of convective storms fall into the anomalous category, with these storms largely confined to the western and upper Great Plains (Zajac & Rutledge, 2001). Even though such storms are rather infrequent, they often contain severe weather (Carey et al., 2003) and therefore are of interest from a severe weather warning perspective. After presenting these three case studies, we synthesize our results by including additional cases to demonstrate that GLM detection efficiency is sensitive to cloud water path, flash height, and flash area. The cases utilized in this study were all obtained in 2017 and utilized data from GOES-16.

2. Data and Methodology

The GLM combines a wide field-of-view lens with a narrow band interference filter, focused on a 1372 × 1300 pixel Charge Coupled Device (CCD) focal plane (Goodman et al., 2013, GOES-R Series Data Book, CDRL PM-14 Rev A. May 2019, NOAA-NASA. Available at https://www.goes-r.gov/downloads/resources/documents/GOES-RSeriesDataBook.pdf). The GLM instrument maps total lightning with a spatial resolution of 8 km at nadir, degrading to 14 km at the limb of the viewing area (Goodman et al., 2013). The 1 nm narrow band interference filter is centered on an oxygen line at 777.4 nm in the spectrum of lightning emissions to accentuate the lightning signal relative to the background (which, during the daytime, also

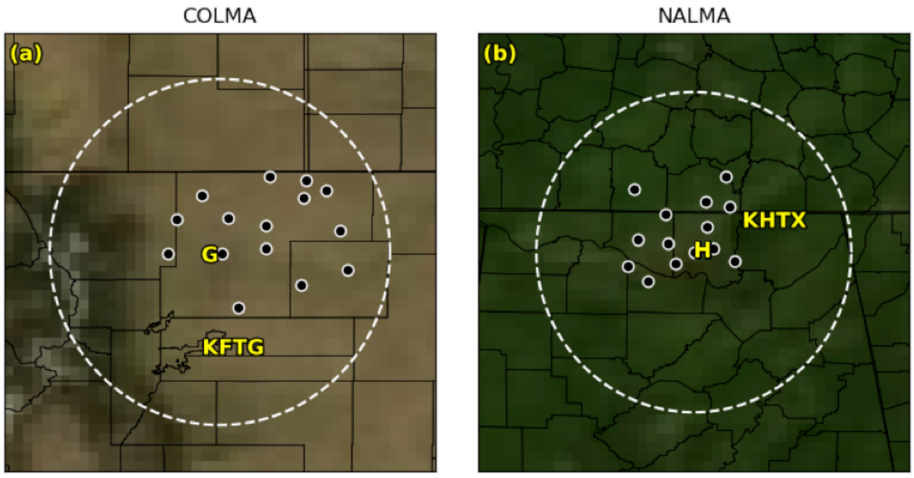

Figure 1. Colorado LMA (a) and North Alabama LMA (b) stations (black circles) that were available during the period of this analysis. A 100 km radius about the nominal LMA center (COLMA: 104.640W, 40.450N and NALMA: 86.645W, 34.724N) is shown (white dashed). The cities of Greeley (G) and Huntsville (H) are labeled.

contains sunlight reflectance). GLM Real-Time Event Processors (RTEPs) use a combination of spatial and temporal filtering to estimate the background scene and separate the lightning signal. The basic unit of data from GLM is termed an "event," which is the integration of all lightning pulses occurring within a nominal 8 × 8 km pixel within a 2 ms integration time window. The operational Lightning Cluster and Filter Algorithm (LCFA) combines simultaneous adjacent illuminated pixels into "groups." The algorithm then clusters groups occurring within 330 ms in time and 16.5 km in space into "flashes." The algorithm also performs requisite filtering to reduce false alarms. The data used in this study are considered pre-operational data (prior to the provisional validation review held in January 2018 at which point the GLM data became available for operational use by forecasters). For completeness and to ensure reproducibility of results, the GOES-16 GLM Beta Validation date was 9 June 2017, the Provisional Validation was 19 January 2018, and Full Validation was 1 November 2018.

Lightning Mapping Arrays (LMA) use a network of sensors to provide the time and location of very high frequency (VHF) sources produced by lightning propagation using time-of-arrival radio direction finding. The location accuracy of LMA data is estimated to be on the order of tens of meters (Thomas et al., 2004), which is obviously much smaller than the GLM pixel size. Two LMA networks are used in our study, the northeast Colorado LMA (COLMA) and the northern Alabama LMA. Figure 1 shows the network of stations in the COLMA (Rison et al., 2012) and the NALMA (Goodman et al., 2005; Koshak et al., 2004). The figure shows a 100 km radius from the center of the LMA network, which is our chosen (conservative) cutoff for using 3-D LMA data. Detection capabilities decrease and source location errors increase dramatically beyond 125 km from the LMA center (Chmielewski & Bruning, 2016; Fuchs et al., 2016; Rison et al., 1999; Thomas et al., 2004), so LMA-based analyses vis-à-vis GLM are confined to this radius.

LMAs detect VHF radio emissions from the discontinuous propagation of lightning channels. As a result, LMAs detect numerous VHF radiation "sources" within each flash and are thus able to provide a satisfactory representation of the spatial extent of a flash. LMAs are considered to have near 100% detection efficiency inside and near the network boundary (Fuchs et al., 2016). In order to obtain flash-level information from LMA data, clustering of the VHF sources is required. This study uses a density-based flash-clustering algorithm (Bruning & MacGorman, 2013; Fuchs et al., 2015, 2016) to cluster the VHF sources spatially and temporally into individual flashes. Sources nominally within 3 km of each other in Colorado (or within 6 km in Alabama) and 150 ms in time (for both LMA) are considered to be part of the same flash. Further, any algorithm-identified flashes must contain 10 or more VHF sources, which has been a common practice when estimating flash rates from LMA networks. The distance between sources criterion (3 km for CO and 6 km for AL) is based in established sensitivity differences between the CO and AL LMA networks (Fuchs & Rutledge, 2018).

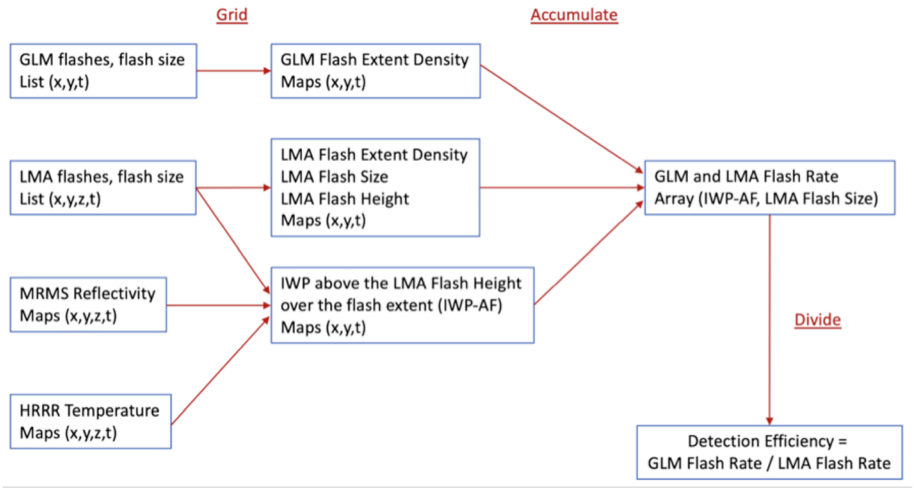

Figure 2. Flow chart illustrating the methodology for computing the detection efficiency.

The use of this LMA density-based flash-clustering algorithm will reduce the GLM detection efficiency, defined as the ratio of GLM flashes to LMA flashes within some time interval over the area of a convective storm, compared to other lightning networks such as Earth Networks ENTLN. We choose to compare the flash rates from GLM against LMA-derived flash rates so that we can also study the covariance of flash rates between the two measurements. For example, if the LMA flash rate varies rapidly in time and the GLM flash rate does not, this would point to challenges with the latter. Furthermore, the LMA flash rates are strongly tied to cloud dynamical and microphysical processes providing additional insights into GLM lightning detection.

Flash rates and flash characteristics are somewhat sensitive to the clustering parameters, algorithm parameters that collect VHF radiation bursts in space and time to construct a flash. However, the range of LMA-derived flash rates obtained by varying the clustering parameters through reasonable ranges is small compared to the absolute difference between LMA and GLM flash rates for the vast majority of the cases we examined. Therefore, the choice of clustering parameters is likely inconsequential to the salient results presented below.

Once the VHF sources are clustered into flashes, several useful lightning flash metrics beside flash rate can be obtained, such as flash size and mean flash height. These metrics are both of high relevance to the present study. The flash size is represented in this study as the flash extent density and also referred to as flash area (Fuchs & Rutledge, 2018). Because LMA location errors are on the order of tens of meters, the flash extent density products can be represented using nearly any grid size, especially that of the GLM pixel size (8× 8 km at nadir). Information about the flash location, especially the mean flash height, has also proven to be useful. Fuchs and Rutledge (2018) showed that LMA-detected lightning flashes in isolated convective storms in Colorado were situated at substantially lower altitudes than comparable storms in central Oklahoma, northern Alabama, and the greater Washington DC area. Note that this crucial piece of information is not available from the GLM instrument. Of particular relevance to the results and discussion to follow, low mean flash heights are a characteristic of anomalous storms (Fuchs & Rutledge, 2018).

The methodology used for evaluating GLM versus LMA is to compare gridded maps of flash extent density. The rationale for this choice is that gridded maps are the form in which most meteorologists will interact with lightning flash data, and lightning flash extent density is one of the lightning variables available on Advanced Weather Interactive Processing System (AWIPS) terminals, used by operational forecasters at National Weather Service (NWS) Weather Forecast Offices (WFOs).

The methodology for creating these maps and calculating DE is given in Figure 2. The GLM observations were resampled to the Multi-Radar Multi-Sensor (MRMS, Zhang et al., 2016) 0.01° cylindrical grid and accumulated over a 6-min period corresponding to three MRMS data file times. We accounted for the difference in area between grid cells in these two regions, which averages 1.012 km^2 for AL and 0.938 km^2 for CO. The

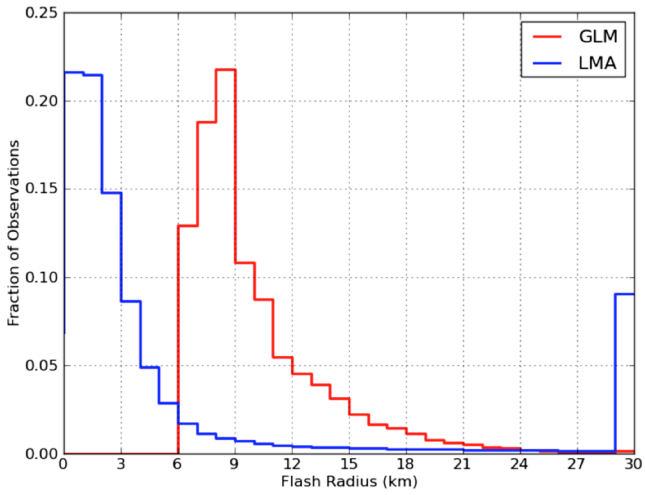

Figure 3. GLM (red) and LMA (blue) flash radii histograms.

resampling assumed the flash extent was a circular area with a 5 km radius. Using the actual flash area from the GLM and LMA data files produced lower correlations than using this fixed value. This may indicate that the flash areas in these two datasets have different physical interpretations arising from their different physical basis of the measurements between GLM and LMA. The LMA flash radius histogram peaks around 2 km, while the GLM histogram peaks around 8 km (Figure 3; dictated by the pixel resolution of GLM). Therefore, 5 km was chosen to split the difference.

Before resampling, location offsets (Table 1) were applied to GLM. Marchand et al. (2019) derived these offsets, which account for the version of the GLM software deployed in operations at the time (a function of date) and location. The offsets are added to the reported GLM location and represent bugs in early pre-operational versions of the GLM algorithm. By 2018, those bugs were fixed, science data and geolocation algorithms were updated, and as a result Marchand et al. (2019) found only small location offsets related to residual parallax displacements.

MRMS radar reflectivity fields at 33 vertical levels, with a spacing ranging from 0.25 km near the ground to 1 km aloft, were used to derive the mean precipitation-sized hydrometeor ice water path (IWP) above individual lightning flashes. In this case, the IWP consists of precipitation-sized particles, as opposed to the cloud IWP retrieved from an optical-spectrum radiometer such as GOES ABI. Cloud particles are beyond the detection limits of 10 cm radars (such as the NEXRAD-88D).

The height of a lightning flash was defined by its geometric mean height. The Carey and Rutledge (2000) relationship was used to estimate the precipitation ice water content (IWC) from the observed radar reflectivity:

$$\mathrm{IWC} = 1000\,\pi\left(\frac{\rho_{\mathrm{ice}}}{\rho_{\mathrm{air}}}\right)N_0^{3/7}\left(\frac{5.28\times10^{-18}Z}{720}\right)^{4/7}$$

where IWC has units of kg m^{-3}, ρ_{ice} is the density of ice (917 kg m^{-3}), ρ_{air} is the density of air in units of kg m^{-3}, N_0 is the intercept parameter of an assumed inverse exponential distribution for ice (taken to be a fixed value 4×10^6 m^{-4}), and Z is the linear radar reflectivity factor at horizontal polarization (units mm^6 m^{-3}).

We also evaluated the Hogan et al. (2006) IWC-Z relationship, which uses a temperature-dependent N_0 value. However, that relationship was trained on stratiform precipitation, and we found unrealistically high IWP results from applying this relationship to deep convection (Figure 4). We did not attempt to separate hydrometeor species in the calculation, as in Carey and Rutledge (2000); however, we did use temperature profiles from the High Resolution Rapid Refresh (HRRR) model to condition the calculation on levels with temperatures below 0°C. The NEXRAD-observed radar reflectivity was reduced by 7.2 dB to account for the difference between the index of refraction of ice and water (Smith, 1984).

The precipitation IWC was integrated vertically upward from the mean LMA flash height and will hereafter be referred to as the Above Flash precipitation IWP (AF-IWP), to a maximum height of 12 (14) km for CO (AL). Above these heights, the MRMS reflectivity profiles began increasing with height because of data sampling issues, and precipitation IWP estimates that included those high altitude echoes exhibited unphysical behavior relative to GLM and LMA flash rates. MRMS composite reflectivity was used to condition the analysis on pixels >35 dBZ (Basarab et al., 2015) to avoid including thunderstorm anvil lightning and stratiform cloud lightning in the analysis.

Thus, in our analysis, each data point represents a sample over a 0.01° × 0.01° area and 6-min time period. Note that three 2-min MRMS data files were averaged together to bring all fields to the same 6-min time resolution. The methodology assumes the precipitation IWP directly

Table 1
Location Offsets Used for GLM Cases (2017)

Cases	Longitude (km)	Latitude (km)
AL: 5/18, 5/24[a], 5/28[a], 6/15	6.6	6.5
CO: 5/8, 5/26, 6/5, 6/12	7.8	10.0
CO: 7/6, 7/29, 8/5, 8/10, 8/15	−8.2	−4.6

[a]Nocturnal cases for which a higher detection efficiency will apply.

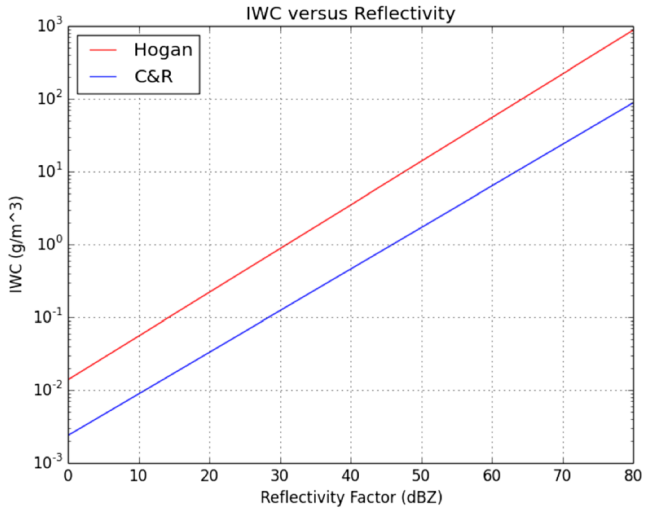

Figure 4. Comparison of Carey and Rutledge (blue) and Hogan et al. (red) IWC relationships at 249 K (at 6 km in a standard atmosphere) with air density 0.660 kg m^{-3}.

above the flash on the rectangular grid is of importance and ignores GLM viewing path effects and 3-D effects such as side-of-cloud illumination. In 2017, GOES-16 was in the test slot at 89.5W, and the satellite zenith angle to COLMA was 49° and to NALMA was 40°, implying the path to COLMA was about 15% longer than to NALMA.

As stated above, the AF-IWP calculated from radar data represents the ice water associated with *precipitation*-sized particles. While precipitation particles have much larger surface areas compared to cloud particles, the latter have far greater concentration, meaning that cloud particles can collectively provide more surface area than precipitation particles for attenuating lighting optical energy (Light et al., 2001; Thomason & Krider, 1982). For example, consider a cloud containing 2 mm diameter precipitation particles with a concentration of 1 L^{-1} and 20 μm diameter cloud particles with concentration of 10^6 L^{-1}. In this case, the cloud particles have ~100× more surface area than the precipitation particles, despite the fact that the mass content from the precipitation particles is 10× greater than the cloud particles. In addition, multiple scattering effects increase the photon path length through the cloud and increase horizontal diffusion away from cloud top, further increasing the attenuation from flash source height to cloud top and thus further suppressing the signal available for GLM detection.

To address possible optical extinction by cloud particles and thus GLM detection efficiency, this study uses retrievals of cloud top path (liquid plus ice) from the GOES ABI. These retrievals are only available during daytime, which reduces our data (a volume around the LMA, every 6 min) from 905 to 539 samples, and examples of the retrievals are shown in Figure 5. The ABI retrieval algorithm (Walther et al., 2013) uses the 0.64 μm (Band 2) and 2.25 μm (Band 6) channels and is based on the classic Nakajima and King (1990) bi-spectral method for simultaneous retrieval of cloud optical depth and cloud-top effective

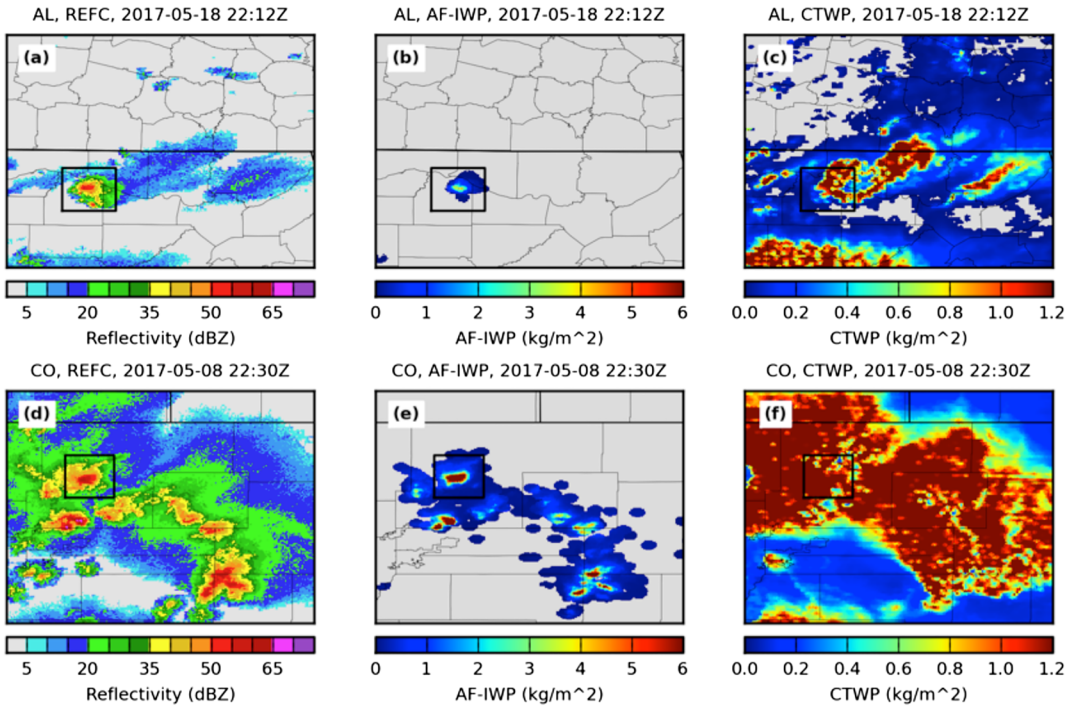

Figure 5. Alabama example showing (a) composite reflectivity, (b) AF-IWP, and (c) CWP. Colorado example showing (d) composite reflectivity, (e) AF-IWP, and (f) CWP. The black box indicates the storm-of-interest in Colorado examined in Figure 6 and Alabama in Figure 8.

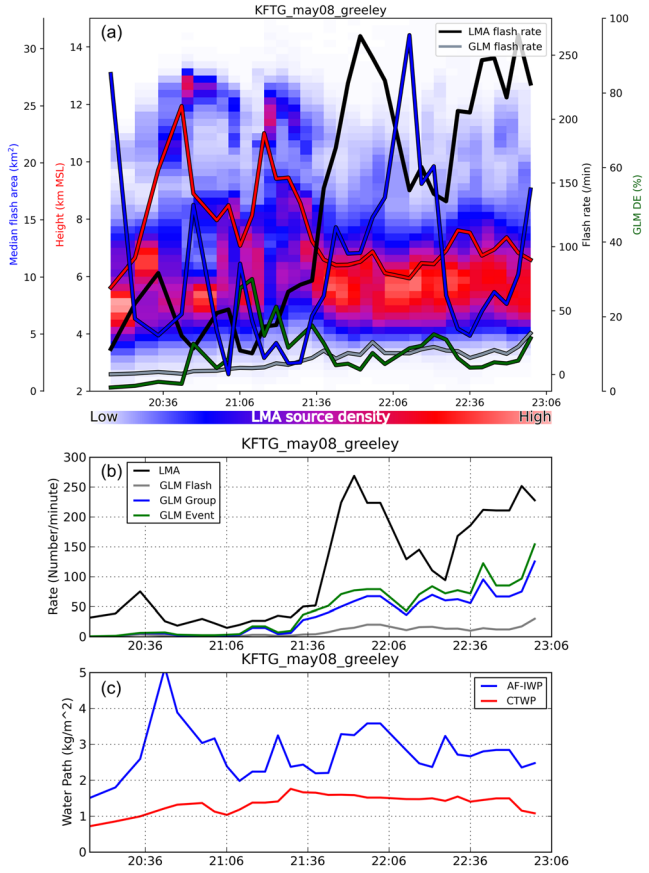

Figure 6. (a) Time series of LMA flash rate, GLM flash rate, median flash area (yellow), median flash height (red), and detection efficiency (green) for an anomalous storm on 8 May 2017 in Colorado observed by the CSU-CHILL radar. The background color shading indicates the sources of VHF burst energy from lightning flashes observed by the CO LMA network. (b) Time series of GLM event (green), group (blue), and flash (gray) rate. (c) Time series of AF-IWP (blue) and CWP (red).

particle size. The ABI on the GOES-16 includes higher spatial resolution and additional near-IR bands, which provide an improvement over the previous imager and allowing for more accurate retrievals.

The ABI estimate of the cloud-top particle size, together with cloud optical depth, is used to estimate the cloud water/ice path (CWP), following parameterizations based on Stephens (1978). The CWP measurement is from the top of the cloud down to a maximum visible-band optical depth of ~160. For Alabama storms that have flashes very high in the cloud, this quantity may provide an accurate estimate of the amount of cloud extinction above the flash. However, for Colorado storms that have flashes substantially lower, this quantity may not probe deep enough to provide a full picture of the "above flash" cloud path. The lack of vertical resolution and saturation in large cloud paths are two well-known inherent limitations of using visible and infrared wavelengths to estimate cloud water path in deep convection. Later, when we present DE versus CWP for AL and CO storm samples, the offsets observed between the AL and CO curves could very well be attributed to this limitation in the ABI cloud path retrieval. That is, the DE for CO storms is systematically lower than the DE in AL storms for the same value of ABI-retrieved CWP, due to this saturation effect. Additionally, it is also worth noting that it is physically impossible to separate these cloud path retrievals between their cloud water and cloud ice components based on ABI retrieval.

3. Case Studies

Three case studies are now examined in order to obtain some basic inferences as to how LMA-derived flash area and flash height correlate with DE, the ratio of the GLM flash rate to the LMA-derived flash rate. Two cases from Colorado (8 May and 10 August 2017) and one from Alabama (18 May 2017) are presented. The Colorado cases are anomalous storms (Bruning et al., 2010; Fuchs et al., 2018). The 8 May storm was observed during the GLM Cal-Val field project carried out in April–May 2017 during post-launch product testing. This storm was in fact overflown by the NASA ER-2 aircraft, although this study did not make use of data obtained from that platform.

Our purpose here is to discuss time series of GLM flash rates, LMA-derived flash rates, LMA-derived flash area, and LMA-derived mean flash height and relate these measurements to DE, defined as the ratio of GLM to LMA flash rates. We also show the source density of LMA points, which is the density of VHF radiation bursts along propagating lightning channels. Regions of high source density coincide with regions of positive charge; therefore, the height of the peak source density is a convenient way to infer if a storm is normal versus anomalous polarity (Fuchs et al., 2015; Fuchs & Rutledge, 2018). In addition to source density, we show time series of GLM group and event rates, from which GLM flashes are distilled. Finally, we plot mean AF-IWP and CWP values for each storm in time series format.

3.1. Case 1: Colorado, 8 May 2017

The 8 May case was part of a storm outbreak that proved to be the costliest weather catastrophe in Colorado history—accounting for $1.4 billion in insured loses, mainly around the greater Denver metropolitan area. Figures 6a–6c show time series of the variables listed above over a 3-hr period from 2000 to 2300 UTC. The period through about 2130 UTC was marked by substantial LMA flash rates of roughly 50 min^{-1}. There are two peaks in flash height within this period, at 2036 and 2115 UTC. These periods are characterized by convective bursts in radar echo depth (overshooting tops), identified by the location of VHF sources near 13 km AGL and mean flash heights above 10 km MSL. Similar features have been discussed by MacGorman et al. (2017).

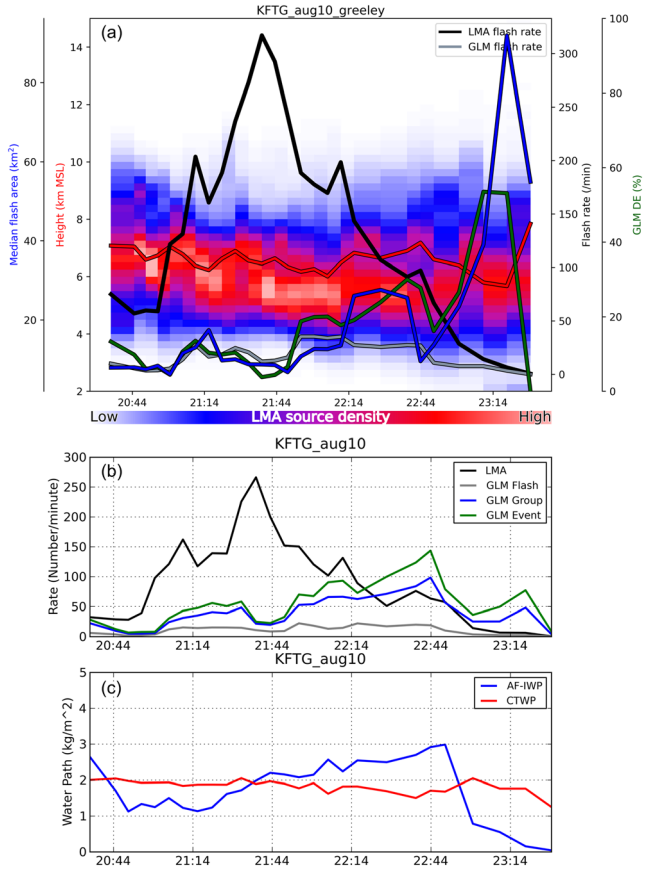

Figure 7. Identical to Figure 6 except for an anomalous storm in Colorado, observed on 10 August 2017. (a) The background color shading indicates the sources of VHF burst energy from lightning flashes observed by the CO LMA network. (b) Time series of GLM event (green), group (blue), and flash (gray) rate. (c) Time series of AF-IWP (blue) and CWP (red).

Although the GLM flash rate is rather modest and has a very small dynamic range, interestingly, there are local "peaks" in GLM DE (~15–35%) that coincide with the overshooting cloud top periods. However, the local increases in DE were caused by reductions in the LMA flash rate, not increases in the GLM flash rate. Evidently, GLM did not detect these elevated flashes, perhaps due to the flashes being very compact (note the trends in mean flash size in Figure 8a). Note that AF-IWP is largest around the period of convective bursts (Figure 6c). After this period, mean flash heights are centered near 6–7 km, and LMA flash rates peak is extreme, peaking over 250 min^{-1} coinciding with low DE, around 10%. Although we only discuss GLM group and event rates casually, we note that the variability in these quantities is more like the variability in LMA flash rate compared to the subdued behavior of GLM flash rate.

Around the peak LMA flash rate (~2156 UTC), GLM DE falls to its lowest value of <10%, when flash heights are centered near 6 km AGL and flash area is also small, ~10 km^2. Low-level VHF source heights and low flash channel heights are again established characteristics of inverted storms (Fuchs & Rutledge, 2018). Although the AF-IWP (radar derived) values are larger than the cloud water path values derived from ABI, it is important to keep in mind that the concentrations of the small particles comprising the cloud path are far more numerous than the particles compromising the AF-IWP. Saturation effects in retrieving CWP, as discussed above, may also be a factor in this case. Below, we will show evidence that the reduced GLM DE is more a function of ABI-derived CWP than AF-IWP; that is, DE is driven by photon scattering of cloud particles opposed to precipitation-sized particles.

3.2. Case 2: Colorado, 10 August 2017

The second case study event occurred on 10 August 2017 storm, featuring another intense, inverted storm in Colorado (Figure 7). Again, we show a time series of roughly 3 hr, similar to Case 1. The storm produced peak flash rates of >300 flashes min^{-1} near 2144 UTC. VHF sources were centered near 6 km AGL, and mean flash heights were tied to this level consistent with the characteristics of inverted storms (Fuchs & Rutledge, 2018). This case illustrates yet another example of an anomalous storm.

Tracking this case with LMA, the broad peak in flash rates is accompanied by compact flashes with areas of roughly 10 km^2. GLM DE values during this intense portion of the storm were generally <20% and unremarkable in dynamic range. Flash areas increase near the end of the observational period when LMA-derived flash rates became small. The storm was beginning to dissipate then, with radar echoes transitioning to a more stratiform structure.

It was noted that GLM DE increased to values approaching 60% as flash sizes increased to 35 km^2 just prior to 2300 UTC. So, even though the mean flash height was still low at this time, it is possible that larger areal flashes were more detectable by GLM. With that said, during the period leading up to 2300 UTC, the LMA flash rate was declining dramatically as well, such that a nearly steady GLM flash rate will artificially augment DE performance. However, this was not verified, and it remains possible that the larger areal flashes had more luminosity allowing detection by GLM. While it is difficult to say anything definitive about the trends in event and group rates, it is noted that during the peak LMA flash rate time both the event and group rates achieved local minimum values (Figure 7b).

Both the AF-IWP and CWP time series remained rather steady during this analysis period, save for decreases at the end of the period associated with storm dissipation (especially for AF-IWP compared to CWP as large precipitation particles fell out of the storm, yet the ice cloud aloft remained; Figure 7c). The 8 May and 10 August cases share common threads during their intense phases, which include compact flashes, low flash

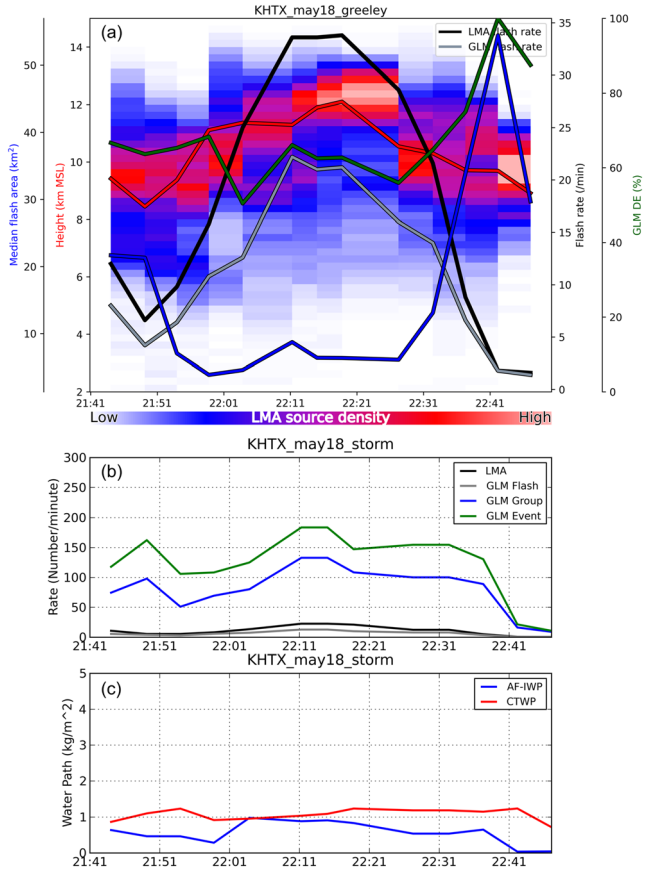

Figure 8. Identical to Figure 7 except for a normal polarity storm in Alabama observed on 18 May 2017. (a) The background color shading indicates the sources of VHF burst energy from lightning flashes observed by the AL LMA network. (b) Time series of GLM event (green), group (blue), and flash (gray) rate. (c) Time series of AF-IWP (blue) and CWP (red).

heights, and consistently large AF-IWP and CWP values. DE values were <20% during the intense phases of both storms.

3.3. Case 3: Alabama, 18 May 2017

The 18 May 2017 Alabama case, being a weaker, normal polarity storm, presents a stark contrast to the two Colorado storm cases. The time series depiction of this case is shown in Figure 8. This case is marked by modest flash rates in comparison to the two previous examples. Interestingly, the flash areas for this modest storm are similar to the previous cases.

The storm intensified between 2203 and 2231 UTC accompanied by an upward shift in VHF sources, corresponding to a slight upward shift in mean flash height. During this intensification period, the LMA flash rate increased by a factor of 3, with the GLM flash rate increasing by a factor of 2. GLM DE values were markedly larger compared to the two previous inverted cases, >60%, which approaches the design GLM DE specification of >70%. GLM DE is slightly lower during the peak lightning period, where we note that mean flash area is at a minimum. Although we do not have an explanation of this behavior, we note that the GLM flash rate in this storm is nearly a factor of 100 smaller than the GLM group rate, implying a significant connectivity among the groups. In other words, many groups are being assembled into the same flash.

The Colorado cases were characterized by very high flash rates (>200 flashes min^{-1}), low flash heights and compact flashes and small GLM DE (~10%), whereas the AL case had modest flash rates (<35 min^{-1}), elevated flash channels, and larger GLM DE (~60–70%). Flash sizes in the AL case were similar to the CO inverted storms. Although it is impossible to draw general conclusions based on this very small sample size, we postulate that the detection of lightning (and associated lightning jumps to indicate pending severe conditions) in anomalous storms may be problematic for the GLM. This finding is consistent with Thomas et al. (2000) who found that LIS-identified cloud-to-ground flashes confined to storm midlevel and lower level were less well detected than intracloud flashes, the latter often extending to storm upper levels. On the other hand, lightning flashes in normal polarity storms, because of their tendency to have flash channels closer to cloud top, are better detected by GLM. Again, this is in agreement with Thomas et al. (2000) who showed that the detection efficiency of LIS identified intracloud discharges improved markedly when the discharges extended into the upper parts of individual storms, where optical depths are less. Similarly, Yoshida et al. (2009) demonstrated a saturation effect in their study of LIS data where clouds of extreme depth were associated with reduced lightning flash rates, which is counterintuitive from the perspective of charge generation.

Comparing Figures 6–8c, the anomalous cases in CO have AF-IWP values roughly four to five times larger than the AL case. Likewise, ABI-retrieved CWP values in the AL case are up to a factor of two smaller compared to those of the CO storms. The AF-IWP values are less in AL because of higher flash channels and reduced ice mass aloft as inferred from radar reflectivity (see Figure 9). In the following section, we provide further evidence and discussion as to the relevance of these parameters in contributing to reductions in DE.

4. Statistical Results

In this section we focus on statistically based analyses. The full set of cases used for the statistical results is listed in Table 1. Again, all cases are from 2017, and all use the GLM on GOES-16 when the satellite was located in its check-out mode position at 89.5°W, prior to drifting to its operational location at 75.2°W. The CO cases occurred during the afternoon and early evening, while two of the four AL cases were mostly or completely nocturnal (see Table 1). We believe these cases are representative of the lightning

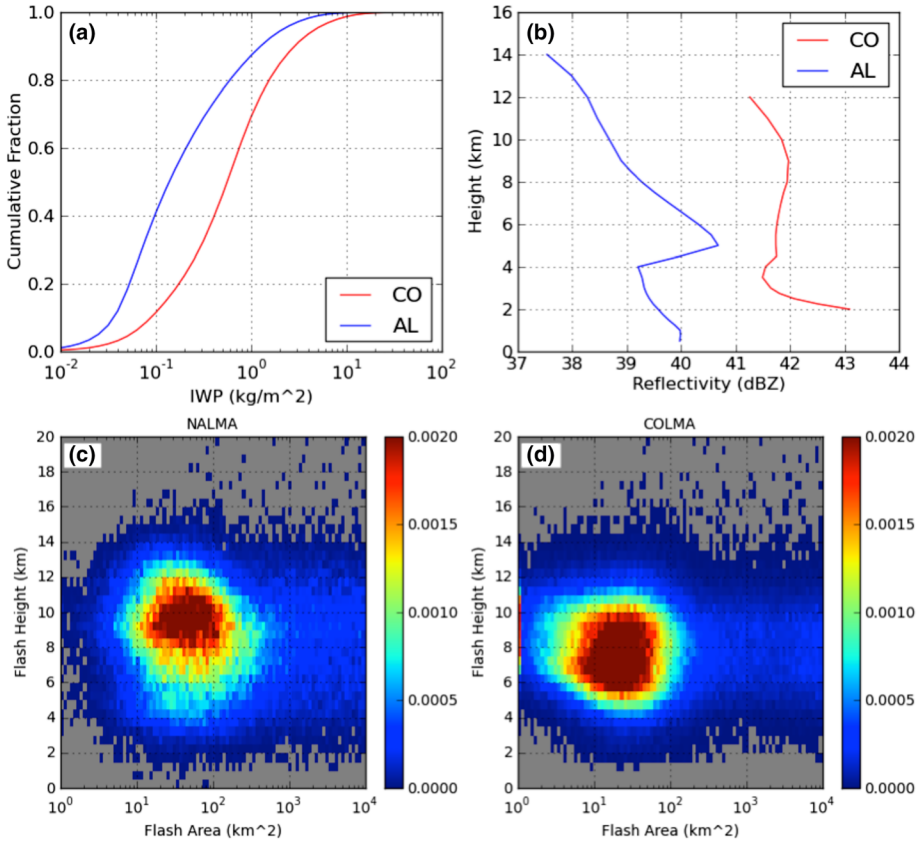

Figure 9. (a) Summary of cases providing the AF-IWP cumulative fraction. (b) Mean profile of radar reflectivity. (c) Joint histogram of flash height (above mean sea level) and flash area for NALMA. (d) As in (c) except for COLMA.

characteristics (flash rates, flash size, and flash heights) associated with deep convection over these two regions. These characteristics were discussed in detail by Fuchs et al. (2015). A higher DE (~10–15%) for the nocturnal AL cases may be expected due to day-night differences in detection (ZC20). Note that the 18 May AL case discussed in the previous section occurred in the late afternoon, so the DE in that case is not subject to day versus night detection differences.

We first consider the microphysical and electrical characteristics of the storms in terms of cumulative distribution (CDF) of precipitation ice water path, mean reflectivity profiles, and 2-D scatter plots of flash area and flash height for the two locations (Figure 9). The CO storms contain larger precipitation IWC as a result of higher radar reflectivity values compared to AL (Figure 9b). These results are consistent with the findings of Fuchs et al. (2015, 2018), which studied larger storm sample sizes. Although CAPE values were not significantly different between the CO and AL storm populations that Fuchs et al. (2015) studied, the higher cloud base heights in CO act to reduce the effects of entrainment, leading to broader and stronger updrafts compared to AL storms. We argue that higher cloud base heights are linked to broader thermals, which are less susceptible to entrainment (Williams & Stanfill, 2002). These updrafts lead to copious amounts of supercooled liquid water and prodigious graupel production. Graupel growing in environments containing high supercooled liquid water contents has been shown to charge positively (Takahashi, 1978, and others). Positively charged graupel leads to the anomalous charge structure.

The stronger updrafts in the CO population (which Fuchs et al., 2018, demonstrated through dual-Doppler radar analysis) lead to larger precipitation ice contents and therefore greater radar reflectivities in the mixed phase region (Figure 9b). Since radar reflectivity varies as D^6 where D is diameter, and precipitation mass M is proportional to D^3, a twofold increase in Z is associated with a fourfold increase in ice mass M (Rutledge et al., 1992). Therefore, modest increases in Z are associated with considerable increases in ice mass and, accordingly, precipitation IWC.

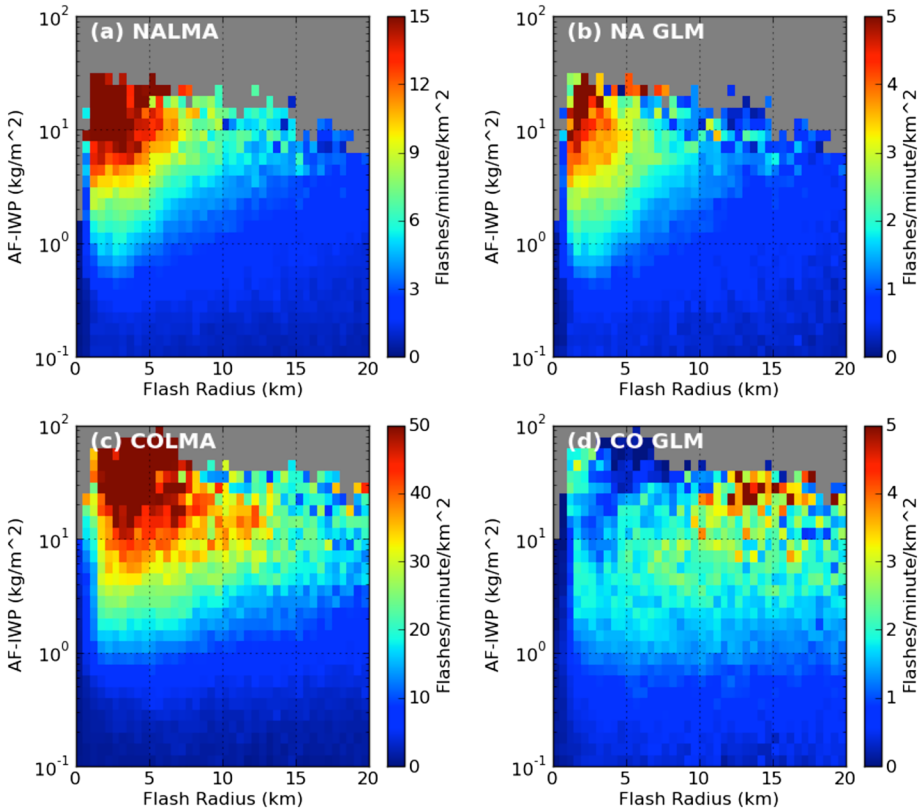

Figure 10. The mean flash rate as a function of AF-IWP and flash radius for NALMA (a), NA GLM (b), COLMA (c), and CO GLM (d). Note the flash rate color bars have different maximum values in each panel.

Turning to statistical plots of flash height versus flash size for the two storm populations (Figures 9c and 9d), the CO events have systematically lower flash heights compared to the AL population. However, there is basically no difference in flash size between AL and CO for the storms we sampled. This observation raises a fundamental question: "Do the lower flash heights in CO, coupled with the larger precipitation ice water contents, cause a reduction in GLM DE?" The lower flash heights in CO coupled with higher ice water contents (inferred from the *Z* profiles in Figure 9b) lead to larger AF-IWP values in CO (Figure 9a). Hence, it is plausible that the higher AF-IWP values in CO lead to lower DE, due to attenuation through scattering of photons emitted by lightning flashes deep in the cloud, a documented characteristic of anomalous storms. This would lead to a reduction in the optical energy emitted from cloud top that could be detected by GLM. A potential takeaway message is that the lower DE in CO is caused by optical attenuation associated with intense precipitation and low flash heights. However, the next two plots contradict this message.

Figure 10 shows the mean flash rates for both the regional LMA and GLM as a function of AF-IWP and flash radius for both regions. First we note that higher flash rates are associated with larger AF-IWP values. This is reasonable, since the precipitation particles contributing to the AF-IWP estimates are a key component of the noninductive charging process (Figures 10a and 10c). Furthermore, the finding of Bruning and MacGorman (2013), that flash size is inversely proportional to flash rate, is clearly evident in our dataset.

A lead that AF-IWP does not explain reduced DE in CO is found in Figures 10b and 10d. In the large AF-IWP/small flash radius portion of these plots (upper left portion of the plots), the peak ratio of LMA/GLM flash rates is near 3:1 in the AL storms (contrast Figures 10a and 10b) compared to over 10:1 for CO storms (contrast Figures 10c and 10d), for similar values of AF-IWP and flash radius. Also, GLM flash rates are higher in AL compared to CO even though the CO LMA flash rates far exceed the AL LMA rates. Figure 11 summarizes estimates of DE as a function of flash radius and AF-IWP. Except for the smallest values of AF-IWP and flash radii, the DE is systematically lower in CO compared to AL, for a given AF-

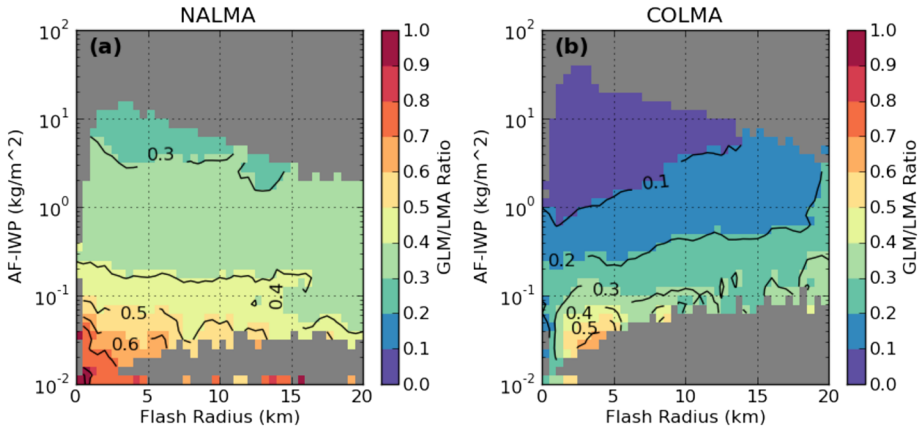

Figure 11. Detection efficiency (GLM/LMA flash rate ratio) versus AF-IWP and flash radius for (a) NALMA and (b) COLMA.

IWP/flash radius couplet. So we conclude that optical scattering by precipitation-sized particles is likely not a viable explanation for the reduced DE in CO.

To pursue a physical explanation for the lower DE in CO, we turn to ABI-based analysis of CWP. The methodology for this estimate was given in section 2. The working hypothesis here is that larger cloud liquid and cloud ice paths (nonprecipitating particles) in CO storms compared to AL storms reduce the DE in CO relative to AL. We base this hypothesis on two points. One, mean flash heights are substantially lower in the CO storms compared to the AL storms analyzed (Figures 9c and 9d). Second, previous research has argued, circumstantially, for enhanced supercooled cloud water in anomalous (CO) storms in comparison to normal polarity storms (Fuchs et al., 2018; Lang & Rutledge, 2002; Williams et al., 2005). Lower flash heights and enhanced supercooled water contents should promote larger cloud paths in CO storms.

Figure 12 shows the relationship between CWP and GLM DE for AL and CO cases. First, DE generally decreases with increasing CWP up to values of 10^{-1} kg m^{-2}. Beyond this value, DE is fairly constant, essentially independent of CWP. Decreasing DE with increasing CWP is consistent with optical scattering by cloud ice particles and cloud water droplets and therefore reduced optical energy at the GLM sensor. To consider further the reduction in DE with increasing CWP, we appeal to previous studies on scattering of photons produced by lightning discharges in clouds, studies such as Thomason and Krider (1982) and Light et al. (2001).

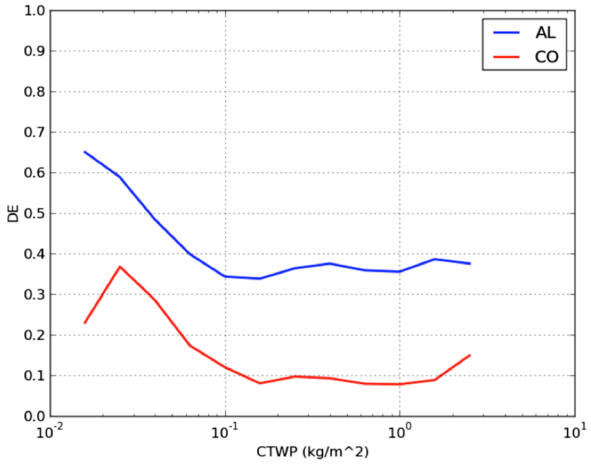

Figure 12. The detection efficiency versus CWP for Alabama (blue) and Colorado (red).

We assume for this discussion that a large CWP corresponds to flashes occurring deep in the cloud, with significant cloud water and cloud ice mixing ratios between the flash and cloud top. The Thomason and Krider results are perhaps the most relevant for this discussion. Following Thomason and Krider, the interaction mean free path of photons (*f*) with a uniform cloud field is inversely proportional to the square of the cloud drop radius and number concentration. For a uniform cloud of depth *L*, the optical depth is then *L*/*f*. For cloud flashes 2 km below cloud top compared to 5 km below cloud top, the optical depth is a factor of 2.5 larger for the deeper flash, implying that the same flash intensity at these levels will be greatly reduced in intensity at cloud top. Baker et al. (1999) developed a model to relate flash rate to several microphysical parameters, including nonprecipitating ice content. They showed that the storm flash rate varied linearly with ice content. If we assume a fixed size for nonprecipitating ice, the flash rate then varies linearly with the concentration of small ice crystals (N_i). For a fourfold increase in flash rate (50 flashes min^{-1}, normal polarity storm vs. 200 flashes min^{-1} anomalous polarity storm), this would result in a fourfold increase in N_i and hence a fourfold increase in extinction due to scattering. The

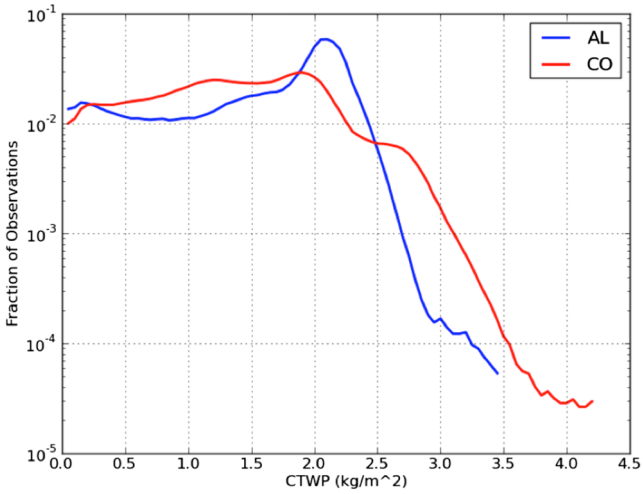

Figure 13. Histograms of ABI cloud top water path for AL (blue) and CO (red) regions.

observation of constant DE at larger values of CWP is more difficult to explain. One possible explanation is that flashes below some critical level are poorly detected by GLM.

Figure 13 shows the distribution of CWP values between AL and CO. The CWP values are essentially the same between the two storm samples, although there is small tail in the CO distribution at larger CWP values. So why are not the CWP values in CO uniformly greater than in AL, since we have made the argument that flashes in the CO storm are lower and cloud mixing ratios are larger? As stated earlier, the ABI calculation is heavily weighted to the cloud top. Therefore, it is quite possible that the CWP estimate is not capturing the variability of intensity in CO.

Returning to Figure 12, there is an obvious offset between the two curves; the DE in AL is larger than the DE in CO for a given CWP value. The offset between the two curves may be caused by the difference in satellite zenith angles between GOES-16 at 89.5W and the viewing area in AL and CO. At the 89.5W location the satellite zenith angle to the AL events is smaller (more nadir) than the zenith angle to CO (more oblique). As demonstrated for TRMM-LIS by Zhang et al. (2019) and K. Cummins (personal communication, U. of Arizona; 20 January 2020), this geometry results in an increase in the minimum detectable optical energy in CO compared to AL by a factor of two or more (i.e., optical emissions in CO flashes require more energy for detection). This sensitivity reduction is caused by a variable pixel size across the GLM CCD. Based on the unpublished analysis of K. Cummins, and further personal communication with E. Bruning (Texas Tech University; 20 January 2020), the zenith angle impact causes a roughly 10% change in GLM DE per fJ increase in energy threshold, which would result in a 20–25% reduction in CO flash detections relative to AL, based purely on geometry. The differences shown in Figure 12 are somewhat larger than this reduction can account for, but it appears that a non-negligible portion of this offset might be attributable to differential viewing geometry. In fact, at the time the data were collected for this study, many estimated detection efficiencies were below the instrument prelaunch predicted DE (>70%). So on a storm-by-storm basis, it is worth noting that even normal polarity storms, with modest LMA-derived flash rates, can have reduced GLM DE relative to the instrument threshold.

5. Conclusions

GLM has ushered in a new era for space-based lightning observations, marking the first such observations from geostationary orbit. The performance of GLM has been shown to be exceptional on a daily and regional basis. The purpose of our study is to comment on GLM performance on an individual storm basis, contrasting normal, and anomalous polarity cases. Although anomalous storms are rather rare in a storm population sense, they are typically severe (Carey et al., 2003), rendering these storms important from a severe warning perspective.

We suggest that the GLM DE is particularly low in anomalous storms due to two main factors, intense cloud water and cloud ice contents and compact flashes at mid-to-low levels in these storms. The large cloud contents increase attenuation of “dim” flashes owing to their compact size. Optical scattering then works to reduce the light intensity at cloud top below GLM detection thresholds. This reasoning is consistent with the modeling study results presented by Brunner and Bitzer (2020) who demonstrated that the light intensity exiting cloud top is sensitive to both the optical emission height (flash height) and the concentration of cloud ice particles between the flash and cloud top. The sensitivity to flash height was particularly true for simulated flash heights below 7 km, which is consistent with mean flash heights in anomalous storms. Our analysis also appears to support the finding that DE is reduced at large zenith viewing angles as the GLM minimum detectable flash energy increases significantly off nadir. So, in some sense, storms in Colorado and more generally convective storms over the western Great Plains are “perfect storms,” in terms of representing the worst-case scenario for GLM detection. Recall Marchand et al. (2019) found low DEs in this same region.

For the anomalous storms, the GLM flash rate shows little if any dynamic range, especially when compared to LMA-derived flash rates. Therefore, it seems a lightning jump signal of updraft intensification (Gatlin & Goodman, 2010; Schultz et al., 2009) would be less useful in these types of storms for identifying developing severe. Although not examined in this study, perhaps GLM group rates would be more useful as input to lightning jump algorithms since group rates have larger dynamic ranges compared to GLM flash rates. It should be noted that reduced DE is not exclusively confined to Great Plains anomalous storms as normal polarity convection in AL show DEs on the order of 40%, consistent with those of ZC20 for storms in Florida. GLM is a revolutionary instrument that will undoubtedly provide for a broad range of operational and scientific applications. The point of this study is simply to identify some storm-dependent issues with detection efficiency and describe the type of storms where reduced DE may be observed.

Data Availability Statement

The L2 GLM data files used in this study are publicly available from NOAACLASS: https://www.avl.class.noaa.gov/saa/products/search?datatype_family=GRGLMPROD. The L1b ABI data files used in this study are publicly available from NOAA CLASS: https://www.bou.class.noaa.gov/saa/products/search?datatype_family=GRABIPRD. The LMA data used in this study can be acquired from New Mexico Tech at http://www.lightning.nmt.edu/nmt_lms/. The Colorado LMA data are available at http://lightning.nmt.edu/colma/. The West Texas LMA data are available at http://pogo.tosm.ttu.edu/about/ The MRMS data used in this study can be acquired from the National Centers for Environmental Prediction (NCEP) at https://mrms.ncep.noaa.gov/data/

Acknowledgments
We thank NOAA for supporting this work, grant number NA19OAR4320073. We thank Matt Rogers at CIRA for processing ABI cloud retrievals for 2017. We also thank Weixin Xu and Karly Reimel for discussions about this work. We also benefitted from discussions with Doug Mach, Ron Thomas, Paul Krehbiel, Ken Cummins, Steve Goodman, Larry Carey, Eric Bruning, and Graeme Stephens.

References

Avila, E. E., & Pereyra, R. G. (2000). Charge transfer during crystal-graupel collisions for two different cloud droplet size distributions. *Geophysical Research Letters*, *27*(23), 3837–3840. https://doi.org/10.1029/2000GL012302

Baker, M. B., Blyth, A. M., Christian, H. J., Latham, J., Miller, K. L., & Gadian, A. M. (1999). Relationships between lightning activity and various thundercloud parameters: Satellite and modelling studies. *Atmospheric Research*, *51*(3–4), 221–236. https://doi.org/10.1016/S0169-8095(99)00009-5

Basarab, B., Rutledge, S. A., & Fuchs, B. (2015). An improved lightning flash rate parameterization from Colorado DC3 thunderstorm data for use in cloud-resolving chemical transport models. *Journal of Geophysical Research: Atmospheres*, *120*, 9481–9499. https://doi.org/10.1002/2015JD023470

Bruning, E. C., & MacGorman, D. R. (2013). Theory and observations of controls of lightning flash size spectra. *Journal of the Atmospheric Sciences*, *70*(12), 4012–4029. https://doi.org/10.1175/JAS-D-12-0289.1

Bruning, E. C., Rust, W. D., MacGorman, D. R., Biggerstaff, M. J., & Schuur, T. J. (2010). Formation of charge structures in a supercell. *Monthly Weather Review*, *138*(10), 3740–3761. https://doi.org/10.1175/2010MWR3160.1

Bruning, E. C., Tillier, C. E., Edgington, S. F., Rudlosly, S. D., Zajic, J., Gravelle, C., et al. (2019). Meteorological imagery for the Geostationary Lightning Mapper. *Journal of Geophysical Research: Atmospheres*, *124*, 14,285–14,309. https://doi.org/10.1029/2019JD030874

Bruning, E. C., Weiss, S. A., & Calhoun, K. M. (2014). Continuous variability in thunderstorm primary electrification and an evaluation of inverted-polarity terminology. *Atmospheric Research*, *135*, 274–284.

Brunner, K. N., & Bitzer, P. M. (2020). A first look at cloud inhomogeneity and its effect on lightning optical emission. *Geophysical Research Letters*, *47*, e2020GL087094. https://doi.org/10.1029/2020GL087094

Carey, L. D., & Rutledge, S. A. (2000). The relationship between precipitation and lightning in tropical island convection: A C-band polarimetric radar study. *Monthly Weather Review*, *128*(8), 2687–2710. https://doi.org/10.1175/1520-0493(2000)128<2687:TRBPAL>2.0.CO;2

Carey, L. D., Rutledge, S. A., & Petersen, W. A. (2003). The relationship between severe storm reports and cloud-to-ground lightning polarity in the contiguous United States from 1989 to 1998. *Monthly Weather Review*, *131*(7), 1211–1228. https://doi.org/10.1175/1520-0493(2003)131<1211:TRBSSR>2.0.CO;2

Chmielewski, V. C., & Bruning, E. C. (2016). Lightning Mapping Array flash detection performance with variable receiver thresholds. *Journal of Geophysical Research: Atmospheres*, *121*, 8600–8614. https://doi.org/10.1002/2016JD025159

Christian, H. J., Blakeslee, R. J., Boccippio, D. J., Boeck, W. L., Buechler, D. E., Driscoll, K. T., et al. (2003). Global frequency and distribution of lightning as observed from space by the Optical Transient Detector. *Journal of Geophysical Research*, *108*(D1), 4005. https://doi.org/10.1029/2002JD002347

Fuchs, B. R., Bruning, E. C., Rutledge, S. A., Carey, L. D., Krehbiel, P. R., & Rison, W. (2016). Climatological analyses of LMA data with an open source lightning clustering algorithm. *Journal of Geophysical Research: Atmospheres*, *121*, 8625–8648. https://doi.org/10.1002/2015JD024663

Fuchs, B. R., & Rutledge, S. A. (2018). Investigation of lightning flash locations in isolated convection using LMA observations. *Journal of Geophysical Research: Atmospheres*, *123*, 6158–6174. https://doi.org/10.1002/2017JD027569

Fuchs, B. R., Rutledge, S. A., Bruning, E. C., Pierce, J. R., Kodros, J. K., Lang, T. J., et al. (2015). Environmental controls on storm intensity and charge structure in multiple regions of the continental United States. *Journal of Geophysical Research: Atmospheres*, *120*, 6575–6596. https://doi.org/10.1002/2015JD023271

Fuchs, B. R., Rutledge, S. A., Dolan, B., Carey, L. D., & Schultz, C. (2018). Microphysical and kinematic processes associated with anomalous charge structures in isolated convection. *Journal of Geophysical Research: Atmospheres*, *123*, 6505–6528. https://doi.org/10.1029/2017JD027540

Gatlin, P. N., & Goodman, S. J. (2010). A total lightning trending algorithm to identify severe thunderstorms. *Journal of Atmospheric and Oceanic Technology*, *27*(1), 3–22. https://doi.org/10.1175/2009JTECHA1286.1

Goodman, S. J., Blakeslee, R. J., Christian, H., Koshak, W., Bailey, J., Hall, J., et al. (2005). The North Alabama lightning mapping array: Recent severe storm observations and future prospects. *Atmospheric Research*, *76*(1–4), 423–437. https://doi.org/10.1016/j.atmosres.2004.11.035

Goodman, S. J., Blakeslee, R. J., Koshak, W. J., Mach, D., Bailey, J., Buechler, D., et al. (2013). The GOES-R Geostationary Lightning Mapper (GLM). *Atmospheric Research*, *125–126*, 34–49. https://doi.org/10.1016/j.atmosres.2013.01.006

Hogan, R. J., Mittermaier, M. P., & Illingworth, A. J. (2006). The retrieval of ice water content from radar reflectivity factor and temperature and its use in evaluating a mesoscale model. *Journal of Applied Meteorology and Climatology*, *45*(2), 301–317. https://doi.org/10.1175/JAM2340.1

Jacobson, A. R., Know, S. O., Franz, R., & Enemark, D. C. (1999). FORTE observations of lightning radio-frequency signatures: Capabilities and basic results. *Radio Science*, *34*(2), 337–354. https://doi.org/10.1029/1998RS900043

Koshak, W. J., Solakiewicz, R. J., Blakeslee, R. J., Goodman, S. J., Christian, H. J., Hall, J. M., et al. (2004). North Alabama lightning mapping array (LMA): VHF source retrieval algorithm and error analyses. *Journal of Atmospheric and Oceanic Technology*, *21*(4), 543–558. https://doi.org/10.1175/1520-0426(2004)021<0543:NALMAL>2.0.CO;2

Kummerow, C., Barnes, W., Kozu, T., Shiue, J., & Simpson, J. (1998). The Tropical Rainfall Measuring Mission (TRMM) sensor package. *Journal of Atmospheric and Oceanic Technology*, *15*(3), 809–817. https://doi.org/10.1175/1520-0426(1998)015<0809:TTRMMT>2.0.CO;2

Lang, T. J., & Rutledge, S. A. (2002). Relationships between convective storm kinematics, precipitation and lightning. *Monthly Weather Review*, *130*(10), 2492–2506. https://doi.org/10.1175/1520-0493(2002)130<2492:RBCSKP>2.0.CO;2

Light, T. E., Suszcynsky, D. M., Kirkland, M. W., & Jacobson, A. R. (2001). Simulations of lightning optical waveforms as seen through clouds by satellites. *Journal of Geophysical Research*, *106*(D15), 17,103–17,114. https://doi.org/10.1029/2001JD900051

Lyons, W. A., Bruning, E. C., Warner, T. A., MacGorman, D. R., Edgington, S., Tillier, C., & Mlynarczyk, J. (2019). Megaflashes: Just how long can a lightning discharge get? *Bulletin of the American Meteorological Society*, *102*, 73–86. https://doi.org/10.1175/BAMS-D-19-0033.2

MacGorman, D. R., Elliott, M. S., & DiGangi, E. (2017). Electrical discharges in the overshooting tops of thunderstorms. *Journal of Geophysical Research: Atmospheres*, *122*, 2929–2957. https://doi.org/10.1002/2016JD025933

Mach, D. M. (2020). Geostationary Lightning Mapping algorithm stability. *Journal of Geophysical Research: Atmospheres*, Special Section: A New Era of Lightning Observations from Space, *125*(5). https://doi.org/10.1029/2019JD031900

Mach, D. M., Christian, H. J., Blakeslee, R. J., Boccippio, D. J., Goodman, S. J., & Boeck, W. L. (2007). Performance of the optical transient detector and lightning imaging sensor. *Journal of Geophysical Research*, *112*, D09210. https://doi.org/10.1029/2006JD007787

Marchand, M., Hilburn, K., & Miller, S. D. (2019). Geostationary Lightning Mapper and Earth Networks lightning detection over the contiguous United States and dependence on flash characteristics. *Journal of Geophysical Research: Atmospheres*, *124*, 11,552–11,567. https://doi.org/10.1029/2019JD031039

Nakajima, T., & King, M. D. (1990). Determination of the optical-thickness and effective particle radius of clouds from reflected solar-radiation measurements. 1. Theory. *Journal of the Atmospheric Sciences*, *47*(15), 1878–1893. https://doi.org/10.1175/1520-0469(1990)047<1878:DOTOTA>2.0.CO;2

Peterson, M. (2019). Research applications for the Geostationary Lightning Mapper operational lightning flash data product. *Journal of Geophysical Research: Atmospheres*, *124*, 10,205–10,231. https://doi.org/10.1029/2019JD031054

Rison, W., Krehbiel, P. R., Thomas, R. J., Rodeheffer, D., Fuchs, B. (2012). The Colorado Lightning Mapping Array. American Geophysical Union Fall Meeting abstract AE23B-0319.

Rison, W., Thomas, R., Krehbiel, P., Hamlin, T., & Harlin, J. (1999). A GPS-based three-dimensional lightning mapping system: Initial observations in central New Mexico. *Geophysical Research Letters*, *26*(23), 3573–3576. https://doi.org/10.1029/1999GL010856

Rudlosky, S. D., Goodman, S. J., & Virts, K. S., (2019). Lightning detection: Geostationary Lightning Mapper, chapter in "The GOES-R series: A new generation of geostationary environmental satellites", Academic Press, Print and e-book, ISBN-13: 978-0128143278, ISBN-10: 0128143274.

Rudlosky, S. D., Goodman, S. J., Virts, K. S., & Bruning, E. C. (2019). Initial Geostationary Lightning Mapper observations. *Geophysical Research Letters*, *46*, 1097–1104. https://doi.org/10.1029/2018GL081052

Rutledge, S. A., Williams, E. R., & Keenan, T. D. (1992). The down under Doppler and electricity experiment (DUNDEE): Overview and preliminary results. *Bulletin of the American Meteorological Society*, *73*(1), 3–16. https://doi.org/10.1175/1520-0477(1992)073<0003:TDUDAE>2.0.CO;2

Saunders, C. P. R., & Peck, S. L. (1998). Laboratory studies of the influence of the rime accretion rate on charge transfer during graupel/crystal collisions. *Journal of Geophysical Research*, *103*(D12), 13,949–13,956. https://doi.org/10.1029/97JD02644

Schmidt, T. J., Griffith, P., Gunshor, M. W., Daniels, J. M., Goodman, S. J., & Lebair, W. J. (2017). A closer look at the ABI on the GOES-R series. *Bulletin of the American Meteorological Society*, *98*(4), 681–698. https://doi.org/10.1175/BAMS-D-15-00230.1

Schultz, C. J., Petersen, W. A., & Carey, L. D. (2009). Preliminary development and evaluation of lightning jump algorithms for the real-time detection of severe weather. *Journal of Applied Meteorology and Climatology*, *48*(12), 2543–2563. https://doi.org/10.1175/2009JAMC2237.1

Smith, P. L. (1984). Equivalent radar reflectivity factors for snow and ice particles. *Journal of Climate and Applied Meteorology*, *23*(8), 1258–1260. https://doi.org/10.1175/1520-0450(1984)023<1258:ERRFFS>2.0.CO;2

Stephens, G. L. (1978). Radiation profiles in extended water clouds. Part II: Parameterization schemes. *Journal of the Atmospheric Sciences*, *35*, 2123–2132.

Takahashi, T. (1978). Riming electrification as a charge generation mechanism in thunderstorms. *Journal of the Atmospheric Sciences*, *35*(8), 1536–1548. https://doi.org/10.1175/1520-0469(1978)035<1536:REAACG>2.0.CO;2

Thomas, R. J., Krehbiel, P. R., Rison, W., Hamlin, T., Boccippio, D. J., Goodman, S. J., & Christian, H. J. (2000). Comparison of ground-based 3-dimensional lightning mapping observations with satellite-based LIS observations on Oklahoma. *Geophysical Research Letters*, *27*(12), 1703–1706. https://doi.org/10.1029/1999GL010845

Thomas, R. J., Krehbiel, P. R., Rison, W., Hunyady, S. J., Winn, W. P., Hamlin, T., & Harlin, J. (2004). Accuarcy of the lightning mapping array. *Journal of Geophysical Research*, *109*, D14207. https://doi.org/10.1029/2004JD004549

Thomason, L. W., & Krider, E. P. (1982). The effects of clouds on the light produced by lightning. *Journal of the Atmospheric Sciences*, *39*(9), 2051–2065. https://doi.org/10.1175/1520-0469(1982)039<2051:TEOCOT>2.0.CO;2

Walther, A., Straka, W., & Heidinger, A. K. (2013). ABI algorithm theoretical basis document for daytime cloud optical and microphysical properties (DCOMP). Version 3.0, 11-June-2013, 66 pp.

Williams, E., Mushtak, V., Rosenfeld, D., Goodman, S., & Boccippio, D. J. (2005). Thermodynamic conditions favorable to superlative thunderstorm updraft, mixed phase microphysics and lightning flash rate. *Atmospheric Research*, *76*(1–4), 288–306. https://doi.org/10.1016/j.atmosres.2004.11.009

Williams, E., & Stanfill, S. (2002). The physical origin of the land-ocean contrast in lightning activity. C.R.–Acad. *Science, Physics*, *3*, 1277–1292.

Yoshida, S., Morimoto, T., Ushio, T., & Kawasaki, Z. (2009). A fifth-power relationship for lightning activity from the Tropical Rainfall Measuring Mission satellite observations. *Journal of Geophysical Research*, *114*, D09104. https://doi.org/10.1029/2008JD01-370

Zajac, B., & Rutledge, S. A. (2001). Cloud-to-ground lightning activity in the contiguous United States from 1995 to 1999. *Monthly Weather Review*, *129*(5), 999–1019. https://doi.org/10.1175/1520-0493(2001)129<0999:CTGLAI>2.0.CO;2

Zhang, D., & Cummins, K. L. (2020). Time evolution of satellite-based optical properties in lightning flashes, and its impact on GLM flash detection. *Journal of Geophysical Research: Atmospheres*. Special Section: A New Era of Lightning Observations from Space, *125*, e2019JD032024. https://doi.org/10.1029/2019JD032024

Zhang, D., Cummins, K. L., Bitzer, P., & Koshak, W. J. (2019). Evaluation of the performance characteristics of the Lightning Imaging Sensor. *Journal of Atmospheric and Oceanic Technology*, *36*(6), 1015–1031. https://doi.org/10.1175/JTECH-D-18-0173.1

Zhang, J., Howard, K., Langston, C., Kaney, B., Qi, Y., Tang, L., et al. (2016). Multi-radar multi-sensor (MRMS) quantitative precipitation estimation: Initial operating capabilities. *Bulletin of the American Meteorological Society*, *97*(4), 621–638. https://doi.org/10.1775/BAMS-D-14-00174.1